

Generation of Paths With Minimum Curvature Derivative With η^3 -Splines

Corrado Guarino Lo Bianco, *Member, IEEE*, and Oscar Gerelli

Abstract—This paper deals with the generation of smooth paths planned by means of η^3 -splines, a recently devised planning primitive used for the automated steering of wheeled mobile robots. The shape of η^3 -splines can be easily modified by acting on a set of free parameters. This capability can be used, for example, to satisfy an assigned optimality criterion. In this paper, it will be used to minimize the curvature variability in order to reduce the lateral solicitations affecting an autonomous robot. Evidently, curvature derivative could be minimized by means of an optimization algorithm. However, this approach cannot be suitably used in an online application which continuously requires the curve updating. For this reason, a heuristic method, based on closed form expressions, has been devised and proposed in the paper in order to efficiently generate almost optimal curves on the sole basis of the interpolating conditions. As a further characteristic, the proposed heuristic expressions permit obtaining, when appropriate interpolating conditions are given, η^3 -splines which at best emulate circular arcs and clothoids.

Note to Practitioners— η^3 -splines represent a powerful tool for the generation of smooth planar paths. Indeed, by means of η^3 -splines it is easily possible to obtain complex composite paths with continuous curvature and curvature derivative. The shape of η^3 -splines can be finely modeled by means of a set of tuning parameters. This positive characteristic poses a practical problem when η^3 -splines have to be used in a real-time framework: the computational burden spent for the parameters tuning must be minimized. The efficient evaluation of such shaping parameters can convert the η^3 -splines from an interesting theoretical tool into a practical, easy-to-use, path generation primitive. The paper investigates this problem and proposes a solution which makes it possible to easily and efficiently generate paths with low curvature derivatives. The final example case shows that, owing to this choice, smooth robot movements, characterized by minimum lateral jerks, can be planned.

Index Terms—Geometric continuity, mobile robots, optimal path generation.

I. INTRODUCTION

SEVERAL approaches can be found in the literature in order to generate appropriate paths for autonomous vehicles. Two different frameworks are normally considered.

Manuscript received January 04, 2008; revised April 04, 2008. First published August 07, 2009; current version published April 07, 2010. This work was recommended for publication by Associate Editor A. S. Kumar and Editor M. Wang upon evaluation of the reviewers' comments. This work is an extended and revised version of a paper presented at the 13th IEEE IFAC International Conference on Methods and Models in Automation and Robotics, MMAR 2007. This work was supported in part by AER-TECH Lab, Emilia Romagna, Italy.

The authors are with the University of Parma, I-43100 Parma, Italy (e-mail: guarino@ce.unipr.it; gerelli@ce.unipr.it).

Color versions of one or more of the figures in this paper are available online at <http://ieeexplore.ieee.org>.

Digital Object Identifier 10.1109/TASE.2009.2023206

In the first one, usually indicated with the name of “motion planning,” a structured and known environment is considered. A path joining two given points is generated taking into account the obstacle avoidance problem and possibly satisfying given constraints. A typical constraint is represented by the maximum path curvature. The first work related to motion planning was due to Dubin [1]: a minimum length path was generated by means of linear segments and circular arcs. Successively, many other works addressed the same problem [2]–[4]. Recently, the problem has been enriched by considering the generation of continuous curvature paths [5].

In the second framework, usually indicated with the term of “motion generation,” the planning phase assumes local characteristics being focused on the generation of short distance paths. This framework is generally encountered when a limited information on the vehicle surroundings is available, such as in the case of a car vehicle moving along an unknown road or an autonomous robot moving inside an environment with strong dynamics characteristics. Obstacle avoidance is generally handled through an opportune choice of the goal point and of the robot final orientation: if a collision is detected, a different target point is selected.

In a motion generation context, path geometric characteristics assume a relevant role. Several path primitives, which generate continuous curvature paths, were proposed in the past: clothoids, cubic spirals [6], polar polynomials [7], intrinsic splines [8], η^2 -splines [9], etc.

Sometimes, curvature continuity is not sufficient to guarantee the generation of smooth robot movements. For example, in [10], it was shown that in order to control an unicycle-like robot by means of continuously differentiable control signals, it is necessary to plan paths whose curvature derivative is continuous. Paths which possess this characteristic are named G^3 -paths. This requirement is not strictly necessary in case of car-like or omnidirectional vehicles, however the use of paths whose curvature is continuously differentiable leads to the generation of smooth command signals, which is, undoubtedly, a positive characteristic [11].

The earlier mentioned η^2 -splines cannot be used to generate G^3 -paths, so that a new planning primitive, named η^3 -spline, has been proposed in [12]. η^3 -splines are evaluated by means of closed form expressions and always fulfill any arbitrarily assigned set of interpolating conditions, including, differently from η^2 -splines, the curvature derivatives on the boundary points. The shape of η^3 -splines can be refined by acting on a set of six freely assignable parameters which do not affect the curve boundary points: the assigned interpolating conditions are always fulfilled independently from the choice of such parameters. Consequently, given an appropriate shaping criterion,

η^3 -splines can be considered a powerful tool for the generation of optimal paths. Two main questions arise: which is the most appropriate optimality criterion to be fulfilled? And, moreover: is it possible to devise the optimal shaping parameters by means of a simple method? There is not a single answer to the first question. Since the control strategy proposed in [10] aims at generating smooth and accurate robot movements, the emphasis has been posed on the generation of paths with reduced curvature derivatives. It will be shown in the paper that, owing to this choice, lateral solicitations acting on a moving vehicle are limited. Curvature derivative can be reduced either by minimizing, along the curve, the integral of its squared values [13] or by minimizing, again along the curve, its maximum values. The two problems are similar but not equivalent. In particular, the first, which can be solved by means of efficient algorithms [14], returns curves whose curvature derivative is on average minimized, but cannot guarantee that spikes of the curvature derivative will not appear in isolated points along the curve, thus causing a control loss. For this reason, the maximum curvature derivative is adopted in this paper as the performance index to be minimized.

Also the answer to the second question is not trivial. If η^3 -splines are used in a motion planning context, the optimal planning problem can be offline solved by means of an algorithm for the global semi-infinite optimization able to manage nonlinear objective functions [15]. This approach is not suited to be used in a motion generation context since, owing to the problem complexity, evaluation times are not compatible with online applications. As a consequence, the solution must be found through a different method. With the help of a program for the global semi-infinite optimization, a heuristic procedure has been devised for the optimal planning of η^3 -splines. Evidently, generated splines are only suboptimal with respect to the proposed optimization problem, but they can be efficiently used in a real-time framework owing to their light computational burden.

In Section II, the G^3 -interpolation problem solved in [12] is recalled (*Problem 1*), and the optimal shaping problem (*Problem 2*), which represents the key point of this paper, is formulated. The proposed solution for *Problem 2* is described in Section III. The results are verified in Section IV by means of a path planning and tracking test case. Final conclusions are drawn in Section V.

II. PROBLEM FORMULATION

A curve in the Cartesian planar space can be described by means of the function

$$\begin{aligned} \mathbf{p} : [u_0, u_1] &\rightarrow \mathbb{R}^2 \\ u \rightarrow \mathbf{p}(u) &= [\alpha(u) \ \beta(u)]^T \end{aligned}$$

where $[u_0, u_1]$ is a real closed interval. The associated “path” is the image of $[u_0, u_1]$ under the vectorial function $\mathbf{p}(u)$, i.e., $\mathbf{p}([u_0, u_1])$. We say that $\mathbf{p}(u)$ is a regular curve if $\dot{\mathbf{p}}(u)$ is piecewise continuous, i.e., $\dot{\mathbf{p}}(u) \in C_p([u_0, u_1])$, and $\dot{\mathbf{p}}(u) \neq 0, \forall u \in [u_0, u_1]$. The arc length or, equivalently, the

curvilinear coordinate measured along $\mathbf{p}(u)$, denoted by s , can be evaluated as

$$\begin{aligned} f : [u_0, u_1] &\rightarrow \mathbb{R} \\ u \rightarrow s &= \int_{u_0}^u \|\dot{\mathbf{p}}(\xi)\| d\xi \end{aligned}$$

where $\|\cdot\|$ indicates the Euclidean norm.

Associated with any point of a regular curve there is a tangent vector $\theta(u)$ measured with respect to the coordinate x -axis, a scalar curvature $\kappa(u)$, and a curvature derivative $\dot{\kappa}(u) := \frac{d\kappa}{ds}(u)$. If $\theta(u)$, $\kappa(u)$, are continuous functions over $[u_0, u_1]$, then $\mathbf{p}(u)$ is a G^2 -curve, i.e., it has a second-order geometric continuity. If also $\dot{\kappa}(u)$ is continuous over $[u_0, u_1]$, then $\mathbf{p}(u)$ has a third-order geometric continuity and is indicated as a G^3 -curve.

In order to control unicycle-like robots by means of continuously differentiable control signals, it is necessary to plan G^3 -curves [10]. A composite G^3 -path can be generated by combining several G^3 -curves if it is possible to assign tangents, curvatures, and curvature derivatives at the extreme points of each of them. This consideration generated the following interpolation problem

Problem 1: Assume that two points $\mathbf{p}_A := [x_A \ y_A]^T$ and $\mathbf{p}_B := [x_B \ y_B]^T$ have been assigned in the Cartesian space. Generate a G^3 -curve $\mathbf{p}(u)$ between \mathbf{p}_A and \mathbf{p}_B which fulfills given interpolating conditions on the initial and final tangent angles θ_A and θ_B , curvatures κ_A and κ_B , and curvature derivatives $\dot{\kappa}_A$ and $\dot{\kappa}_B$.

In order to solve *Problem 1*, a new planning primitive, named η^3 -splines, has been proposed in [12]. It is given by two seven-order polynomial functions defined as follows:

$$\mathbf{p}(u) := [\alpha(u) \ \beta(u)]^T, u \in [0, 1] \quad (1)$$

where

$$\begin{aligned} \alpha(u) &:= \alpha_0 + \alpha_1 u + \alpha_2 u^2 + \alpha_3 u^3 \\ &\quad + \alpha_4 u^4 + \alpha_5 u^5 + \alpha_6 u^6 + \alpha_7 u^7 \end{aligned} \quad (2)$$

$$\begin{aligned} \beta(u) &:= \beta_0 + \beta_1 u + \beta_2 u^2 + \beta_3 u^3 \\ &\quad + \beta_4 u^4 + \beta_5 u^5 + \beta_6 u^6 + \beta_7 u^7. \end{aligned} \quad (3)$$

In the same paper, closed form expressions were proposed in order to efficiently evaluate coefficients α_i and β_i on the basis of the interpolating conditions. From a rapid inspection of the closed form expressions proposed in [12], it is immediately possible to observe that coefficients α_i and β_i depend on the assigned interpolating conditions $x_A, y_A, x_B, y_B, \theta_A, \theta_B, \kappa_A, \kappa_B, \dot{\kappa}_A$, and $\dot{\kappa}_B$ as well as on a set of six real parameters η_i . Such parameters, which give their name to the planning primitive, can be packed into a single vector $\boldsymbol{\eta} := [\eta_1 \ \eta_2 \ \eta_3 \ \eta_4 \ \eta_5 \ \eta_6]^T \in \mathcal{H} \subset (\mathbb{R}^+)^2 \times \mathbb{R}^4$. Among the other characteristics of the η^3 -splines, one, in particular, needs to be highlighted: η^3 -splines always fulfill the boundary conditions independently from the choice of $\boldsymbol{\eta}$. Consequently, vector $\boldsymbol{\eta}$ can be used to shape the curve interior points. This is an important feature of η^3 -splines since it introduces flexibility in their design. On the other hand, it forces to find an appropriate method for the selection of $\boldsymbol{\eta}$. Several

choices are possible. For example, in a motion planning context, $\boldsymbol{\eta}$ could be used to avoid obstacles. In a motion generation context, like that considered in this work, $\boldsymbol{\eta}$ can be used to fulfill an appropriate optimality criterion.

The control strategy developed in [10] and [16] aims at generating smooth robot movements. The path shape has a strong impact on the robot lateral solicitations. In particular, it is well known that lateral accelerations are correlated to the path curvature. In the same way, lateral jerks depend on the curvature derivative with respect to the curvilinear coordinate s . In order to reduce lateral stresses, $\boldsymbol{\eta}$ can be selected by solving the following optimization problem.

Problem 2: Given any set of interpolating conditions $x_A, y_A, x_B, y_B, \theta_A, \theta_B, \kappa_A, \kappa_B, \dot{\kappa}_A$, and $\dot{\kappa}_B$, find the optimal $\boldsymbol{\eta}^3$ -spline which solves the following semi-infinite minimax problem:

$$\min_{\boldsymbol{\eta} \in \mathcal{H}} \max_{u \in [0, 1]} \left\{ \left| \frac{d\kappa}{ds}(u; \boldsymbol{\eta}) \right| \right\} \quad (4)$$

subject to

$$\|\dot{\mathbf{p}}(u; \boldsymbol{\eta})\| > 0, \quad \forall u \in [0, 1]. \quad (5)$$

Constraint (5) is added to guarantee the curve regularity.

Problem 2 is strongly nonlinear and is characterized by a very large number of local minima. For this reason, it can only be solved by means of an algorithm for the global nonlinear optimization. In this paper, the optimal solution is gained by using the hybrid genetic-interval algorithm proposed in [15] and [17]. Unfortunately, this approach can only be adopted for offline cases, since, owing to the problem complexity, evaluation times are normally not compatible with realtime applications. Consequently, it is necessary to devise an efficient heuristic rule to be used when computational efficiency represents an important issue. Such rule, which returns effective solutions and is characterized by an almost zero evaluation time, is described in the next section. In the same section, a comparison is made with a preliminary approach proposed in [12]. In particular, it will be shown how, in most practical cases, the selection method proposed in [12] returns very good results from the point-of-view of problem 2, even if better solutions can be achieved by means of the new approach.

It is worth noticing that the same problem was considered in the past for $\boldsymbol{\eta}^2$ -splines [18]. Also, in that case a heuristic procedure was proposed for the optimal selection of $\boldsymbol{\eta}$. By comparing the two heuristics, it is immediately possible to observe that the solution proposed in [18] has a structure which is much simpler than the one proposed in the next section for $\boldsymbol{\eta}^3$ -splines. This depends on the different characteristics of the two planning primitives. In case of $\boldsymbol{\eta}^2$ -splines, shaping vector $\boldsymbol{\eta}$ is composed by four elements, while it is made of six elements in case of $\boldsymbol{\eta}^3$ -splines. This implies that $\boldsymbol{\eta}^2$ -splines are characterized by less degrees of freedom, so that it is relatively simple to obtain small curvature derivatives. On the contrary, the optimal selection of $\boldsymbol{\eta}$ is much more critical for $\boldsymbol{\eta}^3$ -splines and requires a more complex heuristic selection rule: the curvature derivative can rapidly increase due to a wrong choice of $\boldsymbol{\eta}$.

III. HEURISTIC PROCEDURE

Let us indicate by

$$\begin{aligned} \boldsymbol{\Gamma} &:= [x_A \ y_A \ x_B \ y_B \ \theta_A \ \theta_B \ \kappa_A \ \kappa_B \ \dot{\kappa}_A \ \dot{\kappa}_B]^T \\ &\in \mathcal{G} \subset \mathbb{R}^4 \times [-\pi, \pi]^2 \times \mathbb{R}^4 \end{aligned}$$

the vector containing the interpolating conditions used to plan a generic $\boldsymbol{\eta}^3$ -spline. The minimizer $\boldsymbol{\eta}^*$ of Problem 2 necessarily depends on $\boldsymbol{\Gamma}$, so that it will be indicated in the following as $\boldsymbol{\eta}^*(\boldsymbol{\Gamma})$. In order to avoid an explicit online solution of Problem 2 an algebraic function

$$\begin{aligned} \hat{\boldsymbol{\eta}} &: \mathcal{G} \rightarrow \mathcal{H} \\ \boldsymbol{\Gamma} &\rightarrow \hat{\boldsymbol{\eta}}(\boldsymbol{\Gamma}) \end{aligned}$$

which at the best approximates $\boldsymbol{\eta}^*(\boldsymbol{\Gamma})$, needs to be estimated. Evidently, any effort must be spent in order to guarantee that curves obtained by means of $\hat{\boldsymbol{\eta}}(\boldsymbol{\Gamma})$ have performance indexes close to those obtained by means of $\boldsymbol{\eta}^*(\boldsymbol{\Gamma})$.

A preliminary $\hat{\boldsymbol{\eta}}(\boldsymbol{\Gamma})$ function was proposed in [12]. More precisely, it was selected on the sole basis of the Euclidean norm between \mathbf{p}_A and \mathbf{p}_B according to the following rule:

$$\hat{\boldsymbol{\eta}}(\boldsymbol{\Gamma}) := [\|\mathbf{p}_A - \mathbf{p}_B\| \ \|\mathbf{p}_A - \mathbf{p}_B\| \ 0 \ 0 \ 0 \ 0]^T.$$

In this section, a new $\hat{\boldsymbol{\eta}}(\boldsymbol{\Gamma})$ function, which uses all the interpolating conditions, is designed with the purpose of generating curves with a smaller curvature derivative. The new function $\hat{\boldsymbol{\eta}}(\boldsymbol{\Gamma})$ is obtained through a two steps procedure. The first step aims at devising a possible structure for $\hat{\boldsymbol{\eta}}(\boldsymbol{\Gamma})$. In particular, the structure of $\hat{\boldsymbol{\eta}}(\boldsymbol{\Gamma})$ is obtained by solving Problem 2 for a set of appropriate interpolating conditions $\boldsymbol{\Gamma}_i$ and analyzing the corresponding solutions $\boldsymbol{\eta}^*(\boldsymbol{\Gamma}_i)$. The result of such analysis is a parametric function $\hat{\boldsymbol{\eta}}(\boldsymbol{\Gamma}; \mathbf{k})$, where $\mathbf{k} := [k_1 \ k_2 \ \dots \ k_{11}]^T \in \mathcal{K} \subset \mathbb{R}^{11}$ is a vector of real parameters used for its “tuning.” The first step also returns an initial proposal for \mathbf{k} . Successively, \mathbf{k} is refined in the second step by formulating a new optimization problem.

A. Devising the Structure of $\hat{\boldsymbol{\eta}}(\boldsymbol{\Gamma}; \mathbf{k})$

The structure of $\hat{\boldsymbol{\eta}}(\boldsymbol{\Gamma})$ must be characterized by its simplicity. To this purpose, let us consider some typical planning situations where the solution of problem 2 is known. Evidently, when $\kappa_A = \kappa_B$, the optimal solution of problem 2 is characterized by $\frac{d\kappa}{ds}(u; \hat{\boldsymbol{\eta}}) \simeq 0$, i.e., $\kappa(u; \hat{\boldsymbol{\eta}})$ is kept as constant as possible along the curve or, equivalently, the curve at the best approximates a circular arc. In the same way, if $\kappa_A \neq \kappa_B$, the optimal solution is characterized by a function $\kappa(u; \hat{\boldsymbol{\eta}})$ which almost linearly depends on s , so that $\frac{d\kappa}{ds}(u; \hat{\boldsymbol{\eta}})$ is almost constant and the curve at the best approximates a clothoid. Bearing in mind this idea, a set of interpolating conditions $\boldsymbol{\Gamma}_i$, compatible with arcs and clothoids, has been generated (see Tables I and II).

For each configuration $\boldsymbol{\Gamma}_i$ the optimal solution $\boldsymbol{\eta}^*(\boldsymbol{\Gamma}_i)$ has been found by means of the genetic-interval algorithm proposed in [15], [17]. As expected, in the case of interpolating conditions compatible with circular arcs, problem 2 converges toward solutions with $\frac{d\kappa}{ds} \simeq 0$, i.e., $\boldsymbol{\eta}^3$ -splines almost perfectly emulate circular arcs, while, when interpolating conditions are compatible

TABLE I
INTERPOLATING CONDITIONS Γ_i COMPATIBLE WITH CIRCULAR ARCS

	x_A	y_A	x_B	y_B	θ_A	θ_B	κ_A	κ_B	$\dot{\kappa}_A$	$\dot{\kappa}_B$
Γ_1	0	0	1.4142	0.5858	0	$\pi/4$	1/2	1/2	0	0
Γ_2	0	0	3.5355	1.4645	0	$\pi/4$	1/5	1/5	0	0
Γ_3	0	0	5.3033	2.1967	0	$\pi/4$	1/7.5	1/7.5	0	0
Γ_4	0	0	7.0711	2.9289	0	$\pi/4$	1/10	1/10	0	0
Γ_5	0	0	10.6066	4.3934	0	$\pi/4$	1/15	1/15	0	0
Γ_6	0	0	14.1421	5.8579	0	$\pi/4$	1/20	1/20	0	0
Γ_7	0	0	2.0000	2.0000	0	$\pi/2$	1/2	1/2	0	0
Γ_8	0	0	5.0000	5.0000	0	$\pi/2$	1/5	1/5	0	0
Γ_9	0	0	7.5000	7.5000	0	$\pi/2$	1/7.5	1/7.5	0	0
Γ_{10}	0	0	10.0000	10.0000	0	$\pi/2$	1/10	1/10	0	0
Γ_{11}	0	0	15.0000	15.0000	0	$\pi/2$	1/15	1/15	0	0
Γ_{12}	0	0	20.0000	20.0000	0	$\pi/2$	1/20	1/20	0	0

TABLE II
INTERPOLATING CONDITIONS Γ_i COMPATIBLE WITH CLOTHOIDS

	x_A	y_A	x_B	y_B	θ_A	θ_B	κ_A	κ_B	$\dot{\kappa}_A$	$\dot{\kappa}_B$
Γ_{13}	0	0	2.9511	0.7832	0	$\pi/4$	0	1/2	1.5915e-1	1.5915e-1
Γ_{14}	0	0	7.3776	1.9582	0	$\pi/4$	0	1/5	2.5465e-2	2.5465e-2
Γ_{15}	0	0	11.0664	2.9373	0	$\pi/4$	0	1/7.5	1.1318e-2	1.1318e-2
Γ_{16}	0	0	14.7552	3.9165	0	$\pi/4$	0	1/10	6.3666e-3	6.3666e-3
Γ_{17}	0	0	22.1327	5.8747	0	$\pi/4$	0	1/15	2.8294e-3	2.8294e-3
Γ_{18}	0	0	29.5104	7.8329	0	$\pi/4$	0	1/20	1.5915e-3	1.5915e-3
Γ_{19}	0	0	4.9107	2.7091	0	$\pi/2$	0	1/2	7.9577e-2	7.9577e-2
Γ_{20}	0	0	12.2769	6.7727	0	$\pi/2$	0	1/5	1.2732e-2	1.2732e-2
Γ_{21}	0	0	18.4152	10.1590	0	$\pi/2$	0	1/7.5	5.6588e-3	5.6588e-3
Γ_{22}	0	0	24.5538	13.5454	0	$\pi/2$	0	1/10	3.1831e-3	3.1831e-3
Γ_{23}	0	0	36.8305	20.3181	0	$\pi/2$	0	1/15	1.4147e-3	1.4147e-3
Γ_{24}	0	0	49.1075	27.0909	0	$\pi/2$	0	1/20	7.9577e-4	7.9577e-4

TABLE III
MINIMIZERS $\eta^*(\Gamma_i)$ FOR PROBLEM 2 WHEN INTERPOLATING CONDITIONS ARE CONGRUENT WITH CIRCULAR ARCS

	η_1, η_2	$\eta_3, -\eta_4$	η_5, η_6	$\left \frac{d\kappa^*}{ds} \right $
Γ_1	1.1881e+00	2.3650e+00	-5.7853e+00	2.1210e-05
Γ_2	3.6537e+00	1.3173e+00	-1.0960e+00	4.2403e-06
Γ_3	5.6959e+00	1.0188e+00	-3.7426e+00	1.5579e-07
Γ_4	7.6425e+00	1.4546e+00	-9.3034e+00	5.5453e-07
Γ_5	1.1565e+01	1.2535e+00	-8.9196e+00	4.6852e-08
Γ_6	1.5467e+01	1.3156e+00	-1.0510e+01	2.2694e-08
Γ_7	3.1334e+00	1.0140e-01	-8.4748e+00	2.9981e-05
Γ_8	7.5226e+00	2.0679e+00	-2.1859e+01	5.1968e-06
Γ_9	1.0618e+01	5.6298e+00	-1.5491e+01	8.2154e-07
Γ_{10}	1.5179e+01	1.6468e+00	-2.0441e+01	8.0685e-06
Γ_{11}	2.2828e+01	2.3025e+00	-3.3042e+01	3.3372e-06
Γ_{12}	2.9739e+01	8.4987e+00	-6.3444e+01	9.1094e-07

with clothoids, it converges toward constant values of $\frac{d\kappa}{ds}$ and η^3 -splines approximate clothoids. Moreover, in the case of circular arcs, owing to the symmetry characteristics of such curve ($\kappa_A = \kappa_B$, $\dot{\kappa}_A = \dot{\kappa}_B = 0$), the minimizers are characterized by $\eta_1 \simeq \eta_2$, $\eta_3 \simeq -\eta_4$, and $\eta_5 \simeq \eta_6$. Minimizers $\eta^*(\Gamma_i)$, $i = 1, 2, \dots, 12$, corresponding to circular arcs, are reported in Table III.

In the case of clothoids, η_1 and η_2 are no more equal, but they remain each other close. The same happens for η_3 and $-\eta_4$, and for η_5 and η_6 . For example, for the clothoid whose interpolating conditions are given by Γ_{24} the obtained minimizer is $\eta_1 = 43.8944$, $\eta_2 = 44.8416$, $\eta_3 = 34.2107$, $\eta_4 = -28.1348$, $\eta_5 = -250.1721$, $\eta_6 = -253.6511$. For the sake of conciseness, the set of optimal solutions obtained for clothoids are herein not reported.

TABLE IV
POSSIBLE OPTIMAL PARAMETERIZATIONS FOR (6)–(11)

	\mathbf{k}'	\mathbf{k}''	\mathbf{k}'''
k_1	1	0.986215955980423	0.9900370309156421
k_2	0	0.04694051539639	0.2338305460827709
k_3	0	0.074863997949512	-0.2337321418102114
k_4	0	0.017994903356811	0.0395791203287149
k_5	0	0.233918712355343	0.1008348340478730
k_6	0	0.674868034806584	1.505166060904769
k_7	0	6.17884077781871	0.5363811172337601
k_8	0	-0.062562404082537	-0.5105585534956896
k_9	0	-35.718866041005704	-4.340011523955019
k_{10}	0	65.80182824188454	-17.91610461019005
k_{11}	0	54.58725230016439	-14.14677605082785

By scrutinizing optimal solutions $\eta^*(\Gamma_i)$, it has been possible to devise some correlations between them and the interpolating conditions reported in Tables I and II. Such information has been used to propose the following structure for $\hat{\eta}(\mathbf{T}; \mathbf{k})$:

$$\eta_1 = k_1 \|\mathbf{p}_A - \mathbf{p}_B\| + k_2 |\theta_B - \theta_A| + k_3 \sqrt{|\kappa_A|} \quad (6)$$

$$\eta_2 = k_1 \|\mathbf{p}_A - \mathbf{p}_B\| + k_2 |\theta_B - \theta_A| + k_3 \sqrt{|\kappa_B|} \quad (7)$$

$$\begin{aligned} \eta_3 = & k_4 \|\mathbf{p}_A - \mathbf{p}_B\|^2 + k_5 |\theta_B - \theta_A| + k_6 \sqrt{|\kappa_A|} \\ & + k_7 \sqrt{|\kappa_A|} \end{aligned} \quad (8)$$

$$\begin{aligned} \eta_4 = & - (k_4 \|\mathbf{p}_A - \mathbf{p}_B\|^2 + k_5 |\theta_B - \theta_A| + k_6 \sqrt{|\kappa_B|} \\ & + k_7 \sqrt{|\kappa_B|}) \end{aligned} \quad (9)$$

$$\begin{aligned} \eta_5 = & k_8 \|\mathbf{p}_A - \mathbf{p}_B\|^2 + k_9 \sqrt{|\theta_B - \theta_A|} + k_{10} |\kappa_A| \\ & + k_{11} \sqrt{|\kappa_A|} \end{aligned} \quad (10)$$

$$\begin{aligned} \eta_6 = & k_8 \|\mathbf{p}_A - \mathbf{p}_B\|^2 + k_9 \sqrt{|\theta_B - \theta_A|} + k_{10} |\kappa_B| \\ & + k_{11} \sqrt{|\kappa_B|} \end{aligned} \quad (11)$$

where $\|\cdot\|$ indicates the Euclidean norm and $\mathbf{k} := [k_1 \ k_2 \ \dots \ k_{11}]^T \in \mathcal{K} \subset \mathbb{R}^{11}$ is a vector of real parameters. It is easily possible to verify that, when interpolating conditions are compatible with circular arcs, (6)–(11) correctly return $\eta_1 = \eta_2$, $\eta_3 = -\eta_4$, and $\eta_5 = \eta_6$, while different, but similar, values have to be expected in the case of clothoids. The same selection rule proposed in [12] can be obtained from (6)–(11) by imposing $\mathbf{k} = \mathbf{k}' := [1 \ 0 \ 0 \ 0 \ 0 \ 0 \ 0 \ 0 \ 0 \ 0 \ 0]^T$.

An initial estimate for \mathbf{k} has been found by means of a least square approach which minimizes the differences between $\eta^*(\Gamma_i)$ and $\hat{\eta}(\mathbf{T}_i; \mathbf{k})$, for $i = 1, 2, \dots, 24$. The obtained \mathbf{k} , indicated in the following as \mathbf{k}'' , is shown in Table IV.

B. Estimating the Optimal \mathbf{k}

Starting from \mathbf{k}'' , it is possible to find a more “performing” value of \mathbf{k} . To this purpose, let us introduce the following optimization problem:

$$\min_{\mathbf{k} \in \mathcal{K}} \{\mathbf{J}(\mathbf{k})\} \quad (12)$$

where

$$\mathbf{J}(\mathbf{k}) := \sum_{i=1}^{24} \mathbf{w}_i \left[\frac{d\hat{\kappa}}{ds}(\mathbf{T}_i; \mathbf{k}) - \left| \frac{d\kappa^*}{ds}(\mathbf{T}_i) \right| \right]^2 \quad (13)$$

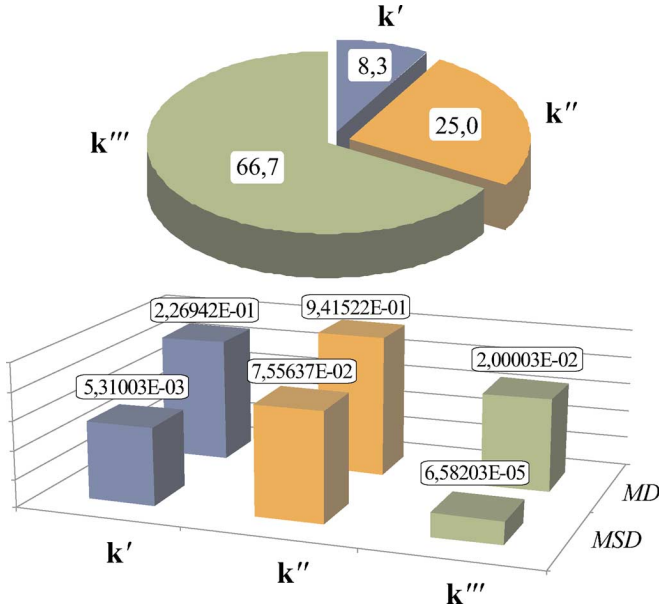


Fig. 1. Comparison between solutions k' , k'' , and k''' in the case of interpolating conditions compatible with circular arcs. The pie diagram reports the percentage of best solutions among k' , k'' , and k''' , while the histogram compares their MSD and their MD . A logarithmic scale has been adopted.

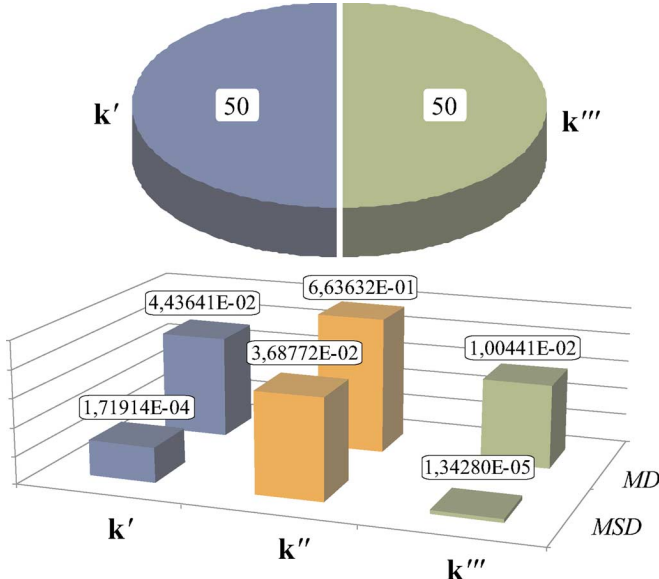


Fig. 2. Comparison between solutions k' , k'' , and k''' in the case of interpolating conditions compatible with clothoids. The pie diagram reports the percentage of best solutions among k' , k'' , and k''' , while the histogram compares their MSD and their MD . A logarithmic scale has been adopted.

and where w_i is a weight assigned to each interpolating condition Γ_i , $\frac{dk}{ds}(\Gamma_i; \mathbf{k}) := \max_{u \in [0,1]} \left\{ \left| \frac{dk}{ds} [u; \hat{\eta}(\Gamma_i; \mathbf{k})] \right| \right\}$ is the maximum curvature derivative obtained by means of $\hat{\eta}(\Gamma_i; \mathbf{k})$, while $\left| \frac{dk^*}{ds}(\Gamma_i) \right|$ represents the maximum curvature derivatives corresponding to the optimal solutions $\eta^*(\Gamma_i)$ of problem 2. The same interpolating conditions Γ_i used for the first phase have been adopted (see Tables I and II). Weights w_i are introduced to take into account the different order of magnitude of minimizer $\eta^*(\Gamma_i)$ (see the last column of Table III). It is worth remembering that $\left| \frac{dk^*}{ds}(\Gamma_i) \right|$ is equal to zero when interpolating conditions are compatible with circular arcs, while it is equal to the

elements of the last column of Table II in the case of clothoids. Practically, the solution of (12) and (13) generates η^3 -splines whose maximum curvature derivative is very close to the minimum achievable for the considered interpolating conditions.

Problem (12), (13) has been solved with a standard optimization algorithm whose starting point was set equal to k'' . The algorithm has converged to solution k''' shown in Table IV, consequently improving the cost index from 5.88589 down to 1.28337e-2.

The effectiveness of k' , k'' , and k''' is discussed in the following with the help of two performance indexes. In particular, we define mean squared deviation (MSD) the mean, evaluated over all the interpolating conditions Γ_i , of the squared differences between $\frac{dk}{ds}(\Gamma_i; \mathbf{k})$ and $\left| \frac{dk^*}{ds}(\Gamma_i) \right|$, that is

$$MSD = \frac{1}{n} \sum_i \left[\frac{dk}{ds}(\Gamma_i; \mathbf{k}) - \left| \frac{dk^*}{ds}(\Gamma_i) \right| \right]^2 \quad (14)$$

where $\mathbf{k} = k', k'', k'''$, while n is the number of considered interpolating conditions Γ_i . In the same way, we define maximum deviation (MD) the following index:

$$MD = \max_i \left\{ \frac{dk}{ds}(\Gamma_i; \mathbf{k}) - \left| \frac{dk^*}{ds}(\Gamma_i) \right| \right\} \quad (15)$$

i.e., the maximum difference, evaluated over a set of interpolating conditions Γ_i , between the optimal cost indexes and those obtained by means of (6)–(11).

Fig. 1 shows some statistic results concerning circular arcs. They have been evaluated by considering the set of interpolating conditions of Table I. The pie diagram shows the percentage of best solutions, from the point-of-view of the curvature derivative, among k' , k'' , and k''' . In 66.7% of cases, k''' exhibits the smallest cost index. The histogram in the same figure compares k' , k'' , and k''' by means of (14) and (15), assuming $i = 1, \dots, 12$, $n = 12$, and $\left| \frac{dk^*}{ds}(\Gamma_i) \right| = 0$. Also in this case k''' represents the best solution since the MSD and the MD indexes are, respectively, one-order and two-orders of magnitude smaller than those obtained for k' .

In the case of clothoids, the comparisons are shown in Fig. 2. The pie diagram evidences how best solutions are equally spread among k' and k''' . Nevertheless, some further conclusions can be drawn from the histogram. It has been evaluated by considering $i = 13, \dots, 24$ and $n = 12$. Necessarily, terms $\left| \frac{dk^*}{ds}(\Gamma_i) \right|$ depend on the interpolating conditions Γ_i (see the last column in Table II). The histogram reveals that the MSD and the MD indexes of k''' are evidently better than those of k' . The reason of this result is that when k' is characterized by the best cost indexes, k''' has worst but similar performance indexes, while when k''' returns the best solutions they are neatly better than those proposed by k' .

Owing to the method used for selecting \mathbf{k} , function $\hat{\eta}(\Gamma; \mathbf{k}')$ generates curves which very well approximate circular arcs and clothoids. It could be interesting to verify what happens in the case of generic interpolating conditions. To this purpose, 30 interpolating conditions Γ_i have been randomly chosen belonging to the following intervals: $x_B \in [0, 15]$, $y_B \in [-5, 5]$, $\theta_B \in [-\pi/2, \pi/2]$, $\kappa_A, \kappa_B \in [-0.4, 0.4]$, $\dot{\kappa}_A, \dot{\kappa}_B \in [-0.04, 0.04]$. Without any loss of generality, it has been supposed that $x_A =$

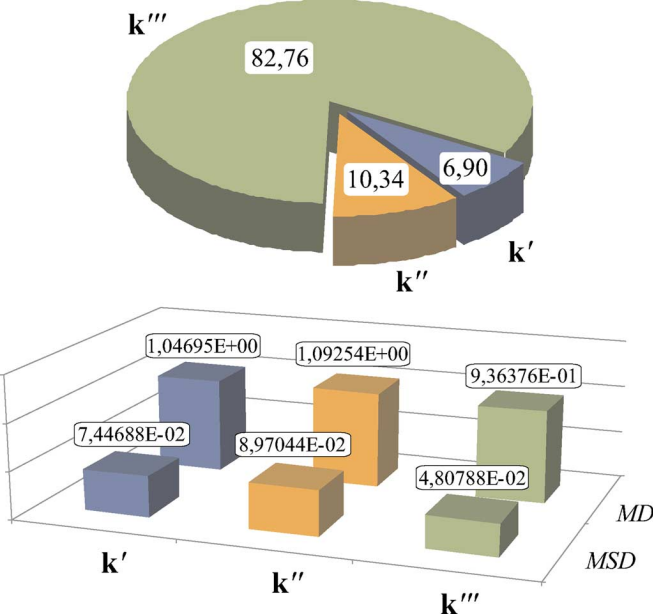


Fig. 3. Comparison between solutions k' , k'' , and k''' in the case of generic interpolating conditions. The pie diagram reports the percentage of best solutions among k' , k'' , and k''' , while the histogram compares their MSD and their MD. A logarithmic scale has been adopted.

$x_B = \theta_A = 0$ since, according to (6)–(11), terms η_i are evaluated on the sole basis of differences $\mathbf{p}_B - \mathbf{p}_A$ and $\theta_B - \theta_A$.

For each value of Γ_i an optimal solution $\boldsymbol{\eta}^*(\Gamma_i)$ has been obtained by solving problem 2 with the genetic-interval algorithm. The resulting cost indexes $\left| \frac{d\kappa^*}{ds}(\Gamma_i) \right|$ have been compared with the performance indexes $\frac{d\kappa}{ds}(\Gamma_i; \mathbf{k})$ evaluated for k' , k'' , and k''' . The pie diagram of Fig. 3 shows that k''' can be considered the best solution in the 83% of cases. Nevertheless, k' and k'' have comparable performance indexes, as can be deduced from the histogram in the same figure. This conclusion is also confirmed by $J(\mathbf{k})$: for the three cases it is respectively equal to $J(\mathbf{k}') = 2.1596$, $J(\mathbf{k}'') = 2.6015$, and $J(\mathbf{k}''') = 1.3943$. Fig. 4 further proves this assertion by showing a direct comparison, for 7 of the 30 analyzed cases, between the maximum curvature derivatives obtainable with the three proposed methods and those returned by the genetic-interval algorithm. In any situation, the best solutions are those devised by the genetic-interval algorithm, but the performance indexes of k' , k'' , and k''' are each other comparable and very close to those of the actual minimizers.

Some conclusions can be drawn from the comparisons. Generally, k''' generates the smallest curvature derivatives. Even when k' or k'' are characterized by smaller curvature derivatives, the performance indexes of k''' are only slightly worse. In the case of generic interpolating conditions k' , k'' , and k''' can be considered equivalent: this result proves that the method originally proposed in [12] for the selection of $\boldsymbol{\eta}$ represents a sufficiently good solution for problem 2.

One final doubt is instilled by Fig. 4. It seems that, in the case of generic interpolating conditions, the selection of $\boldsymbol{\eta}$ is not particular critical since the cost indexes of k' , k'' , and k''' are each other comparable and close to those of the global optimal solutions. This is not true, as can be evinced from the example case

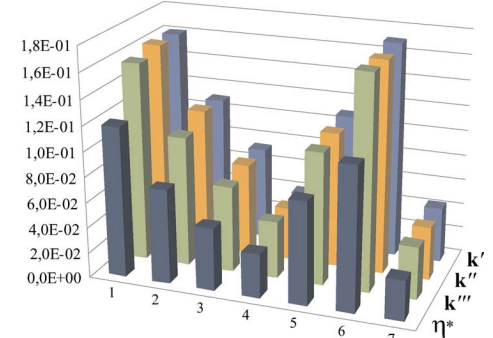


Fig. 4. Comparison between the performance indexes of $\boldsymbol{\eta}^*$, k' , k'' , and k''' for seven generic sets of interpolating conditions. A linear scale has been adopted.

TABLE V
INTERPOLATING CONDITION Γ_i CHOSEN FOR THE EXAMPLE CASES

	x_A	y_A	x_B	y_B	θ_A	θ_B	κ_A	κ_B	$\dot{\kappa}_A$	$\dot{\kappa}_B$
Γ_{25}	0	0	4.10	1.66	0	$3\pi/8$	0	$1/2$	0.106	0.106
Γ_{26}	4.10	1.66	7.00	10.00	$3\pi/8$	0	$1/2$	-0.1	0.106	0
Γ_{27}	7.00	10.00	14.07	7.07	0	$-\pi/4$	-0.1	-0.1	0	0
Γ_{28}	14.07	7.07	15.40	5.00	$-\pi/4$	$-5\pi/8$	-0.1	0	0	0
Γ_{29}	15.40	5.00	15.78	4.08	$-5\pi/8$	$-5\pi/8$	0	0	0	0

proposed in the next section where the $\boldsymbol{\eta}$ -parameters obtained from (6)–(11) and k''' are slightly perturbed, thus causing an immediate rise of $\dot{\kappa}$.

IV. APPLICATION CASE

The example case proposed in the following points out the influence exerted by the curvature derivative on the motion performances of a mobile robot. Let us consider an unicycle mobile robot which must move along a composite curve planned by means of $\boldsymbol{\eta}^3$ -splines. The interpolating conditions used for the generation of the $\boldsymbol{\eta}^3$ -spline paths are listed in Table V. In more detail, the interpolating conditions Γ_{25} , Γ_{27} , and Γ_{29} are compatible with a clothoid, a circular arc and a linear segment respectively, while interpolating conditions Γ_{26} and Γ_{28} are not compatible with any standard planning primitive in order to emulate a set of actual data obtained, e.g., from a visual system. It can be immediately evinced from Table V that the interpolating conditions of each partial curve, i.e., initial and final tangents, curvatures, and curvature derivatives, are selected such to guarantee the required G^3 -continuity of the overall composite path.

In order to verify the relevance of designing curves with minimum curvature derivative, three different scenarios have been considered. In the first case, indicated in the following as the nominal case, the $\boldsymbol{\eta}$ parameters are evaluated by means of (6)–(11) and coefficients k''' shown in Table IV. In the second and in the third case, the perturbed cases, the previously evaluated $\boldsymbol{\eta}$ -parameters are slightly modified. More precisely, η_1 and η_2 have been increased and decreased, respectively, by the 10% with respect to the nominal case. As a result, three different composite curves satisfying the assigned interpolating conditions have been generated. It is possible to evince from Fig. 5 that the three curves have a very similar shape, but a comparison between Figs. 6 and 7, which report κ and $\dot{\kappa}$ for the nominal case and one of the two modified cases, highlights how the small perturbations introduced in η_1 and η_2 produce

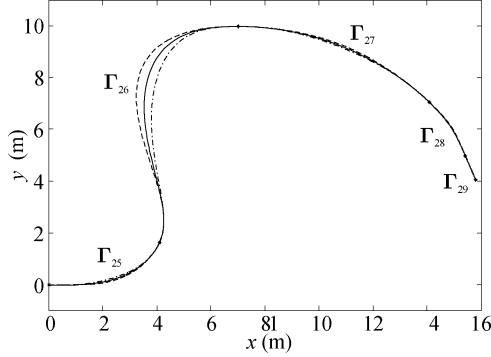


Fig. 5. Nominal path (continuous curve) compared with the paths obtained increasing (dashed line) or decreasing (dash-dotted line) η_1 and η_2 by the 10%.

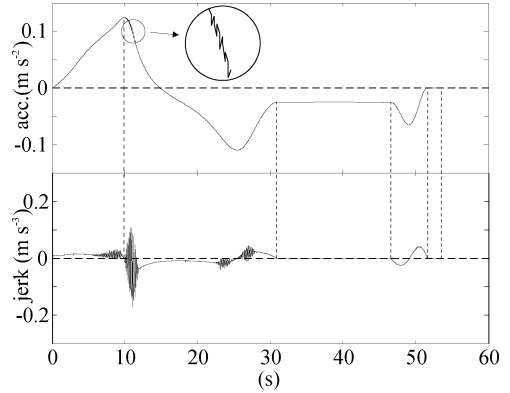


Fig. 8. Lateral acceleration and jerk along the nominal curve.

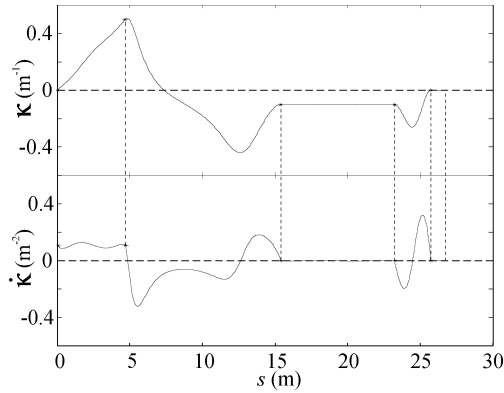


Fig. 6. Path curvature and its first derivative for the nominal case.

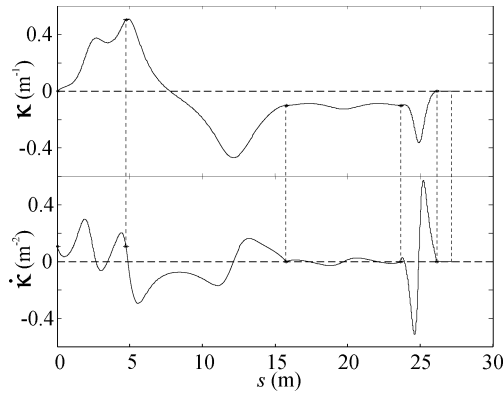


Fig. 7. Path curvature and its first derivative obtained increasing η_1 and η_2 by the 10%.

evident changes in the curvature and in the curvature derivative. Fig. 6 highlights the better emulation of clothoids and circular arcs obtained in the nominal case: differently from the perturbed scenario, the curvature derivative is almost constant. As expected, $\dot{\kappa}$ is generally higher in the perturbed case. The situation worsens especially in the case of Γ_{28} , thus demonstrating how the selection of η can be very critical also when generic interpolating conditions are considered.

To better point out the differences between the three composite curves, they have been tracked by an unicycle-like mobile robot driven accordingly to the control strategy proposed

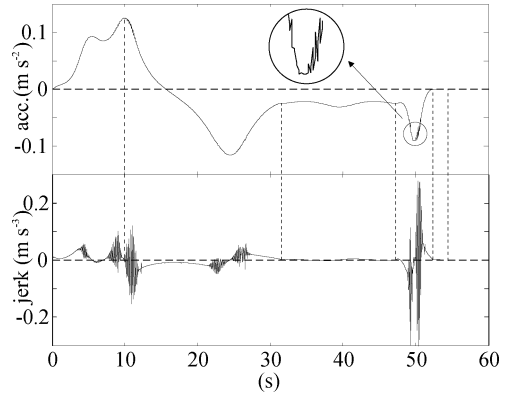


Fig. 9. Lateral acceleration and jerk obtained increasing η_1 and η_2 by the 10%.

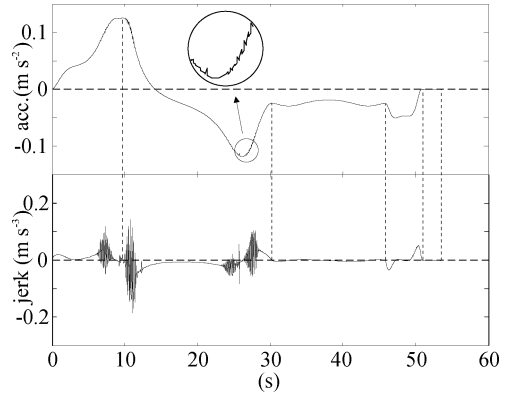


Fig. 10. Lateral acceleration and jerk obtained decreasing η_1 and η_2 by the 10%.

in [10]. The robot model used for the simulations takes into account the vehicle dynamics and the existence of sliding effects between wheels and ground. To this purpose, the wheels traction model originally proposed in [19] has been adopted. The vehicle moves at a constant longitudinal velocity, thus the shape of the lateral acceleration is similar to the curvature shape, while the jerk profile mimics the curvature derivative profile. Fig. 8 shows the lateral acceleration and the lateral jerk acting on the vehicle during its movement along the nominal path. The detail in the same figure reveals how the lateral skidding phenomenon can appear every time lateral accelerations and jerks are sufficiently high. As previously asserted, lateral jerk is directly correlated to the curvature derivative and, consequently, the nominal case

is characterized by smaller lateral solicitations, being an almost optimal solution for problem 2. On the contrary, Fig. 9 reveals that if η_1 and η_2 are increased, the lateral skidding phenomenon can more easily appear owing to the higher lateral stresses acting on the vehicle. The situation does not improve when η_1 and η_2 are decreased with respect to the optimal values, as can be evinced from Fig. 10.

V. CONCLUSION

Smart planar curves, suited for autonomous robots, can be generated by means of η^3 -splines. Acting on a vector η of freely tunable parameters, it is possible to shape η^3 -splines such to fulfill a given optimality criterion. The selection of η represents a key point for the generation of optimal paths: a wrong choice can easily introduce undesired vehicle solicitations. In particular, it has been shown how, by acting on η , it is possible to generate curves with minimum curvature derivative with the purpose of minimizing the vehicle lateral jerk. In order to avoid the execution of huge online optimizations, a heuristic method has been proposed for the suboptimal selection of η . When interpolating conditions are compatible with circular arcs and clothoids, the devised expressions generate curves which at the best emulate such primitives. In the case of generic interpolating conditions, the curvature derivative is very close to the actual achievable minimum.

REFERENCES

- [1] L. Dubins, "On curves of minimal length with a constraint on average curvature and with prescribed initial and terminal positions and tangents," *Amer. J. Math.*, vol. 79, pp. 497–517, 1957.
- [2] J. Reeds and R. Shepp, "Optimal paths for a car that goes both forward and backward," *Proc. Amer. Math. Soc.*, vol. 145, no. 2, pp. 367–393, 1990.
- [3] J.-D. Boissonnat, A. Cérézo, and J. Leblond, "Shortest paths of bounded curvature in the plane," in *Proc. 1992 IEEE Int. Conf. Robot. Autom.*, Nice, France, May 1992, pp. 2315–2320.
- [4] P. Souères and J.-P. Laumond, "Shortest paths synthesis for a car-like robot," *IEEE Trans. Autom. Control*, vol. 41, no. 5, pp. 672–688, May 1996.
- [5] T. Fraichard and A. Scheuer, "From Reeds and Shepp's to continuous-curvature paths," *IEEE Trans. Robot.*, vol. 20, no. 6, pp. 1025–1035, Dec. 2004.
- [6] Y. Kanayama and B. Hartman, "Smooth local path planning for autonomous vehicles," in *Proc. IEEE Int. Conf. Robot. Autom.*, *ICRA89*, Scottsdale, AZ, May 1989, vol. 3, pp. 1265–1270.
- [7] W. Nelson, "Continuous-curvature paths for autonomous vehicles," in *Proc. IEEE Conf. Robot. Autom.*, Scottsdale, AZ, May 1989, vol. 3, pp. 1260–1264.
- [8] H. Delingette, M. Hébert, and K. Ikeuchi, "Trajectory generation with curvature constraint based on energy minimization," in *Proc. IEEE-RSJ Int. Conf. Intell. Robot. Syst.*, Osaka, Japan, Nov. 1991, pp. 206–211.
- [9] A. Piazz and C. Guarino Lo Bianco, "Quintic G^2 -splines for trajectory planning of autonomous vehicles," in *Proc. IEEE Intel. Veh. Symp.*, Dearborn, MI, Oct. 2000, pp. 198–203.
- [10] C. Guarino Lo Bianco, A. Piazz, and M. Romano, "Smooth motion generation for unicycle mobile robots via dynamic path inversion," *IEEE Trans. Robot.*, vol. 20, no. 5, pp. 884–891, Oct. 2004.
- [11] J. Reuter, "Mobile robots trajectories with continuously differentiable curvature: An optimal control approach," in *Proc. IEEE/RSJ Int. Conf. Intell. Robot. Syst.*, Victoria, B.C., Canada, Oct. 1998, vol. 1, pp. 38–43.
- [12] A. Piazz, C. Guarino Lo Bianco, and M. Romano, " η^3 -splines for the smooth path generation of wheeled mobile robots," *IEEE Trans. Robot.*, vol. 23, no. 5, pp. 1089–1095, 2007.
- [13] H. Moreton, "Minimum curvature variation curves, networks, and surfaces for fair free-formshape design," Ph.D. dissertation, Univ. California, Berkeley, CA, 1992.
- [14] J. Shinn-Hwa Wang and W. Wei-Ming Dai, "Transformation of min-max optimization to least-square estimation and application to interconnect design optimization," in *Proc. IEEE Int. Conf. Comput. Des.*, *ICCD'95*, Austin, TX, Oct. 1995, pp. 664–670.
- [15] C. Guarino Lo Bianco and A. Piazz, "A hybrid algorithm for infinitely constrained optimization," *Int. J. Syst. Sci.*, vol. 32, no. 1, pp. 91–102, Jan. 2001.
- [16] C. Guarino Lo Bianco, "Optimal velocity planning for autonomous vehicles under kinematic constraints," in *Proc. 8th Int. IFAC Symp. n Robot Control*, *SYROCO 2006*, Bologna, Italy, Sep. 2006.
- [17] C. Guarino Lo Bianco and A. Piazz, "A hybrid genetic/interval algorithm for semi-infinite optimization," in *Proc. 35th Conf. Decision and Control*, Kobe, Japan, Dec. 1996, pp. 2136–2138.
- [18] C. Guarino Lo Bianco and A. Piazz, "Optimal trajectory planning with quintic G^2 -splines," in *Proc. IEEE Intell. Veh. Symp. IV 2000*, Dearborn, MI, Oct. 2000, pp. 620–625.
- [19] H. Dugoff, P. S. Fancher, and L. Segel, "An analysis of tyre traction properties and their influence on vehicle dynamic performance," in *Proc. SAE*, 1970, pp. 1219–1243, Paper No. 700377.



Corrado Guarino Lo Bianco (M'05) received the Degree in electronic engineering (Hon) and the Ph.D. degree in control system engineering from the University of Bologna, Bologna, Italy, in 1989 and 1994, respectively.

Currently, he is with the Dipartimento di Ingegneria dell'Informazione, University of Parma, Parma, Italy, as an Aggregate Professor of Industrial Robotics. He is involved in research concerning mobile and industrial robotics. In particular, he is mainly interested in topics concerning the smooth and optimal trajectory generation, robot kinematics and dynamics, and robot control.



Oscar Gerelli was born in Piacenza, Italy, in 1981. He graduated with honors in computer engineering in 2005 from the University of Parma, Parma, Italy. He is currently working towards the Ph.D. degree from University of Parma.

In 2007, he spent two quarters at the University of Twente, Enschede, The Netherlands, as a visiting student. Currently, he is involved in research on smooth profile generation for motion control and in optimal control algorithms for linear and nonlinear systems.